



HAL
open science

Maturation of PNN and ErbB4 Signaling in Area CA2 during Adolescence Underlies the Emergence of PV Interneuron Plasticity and Social Memory

Soledad Domínguez, Christophe Clément Rey, Ludivine Therreau, Aurélien Fanton, Dominique Massotte, Laure Verret, Rebecca Ann Piskorowski, Vivien Chevaleyre

► To cite this version:

Soledad Domínguez, Christophe Clément Rey, Ludivine Therreau, Aurélien Fanton, Dominique Massotte, et al.. Maturation of PNN and ErbB4 Signaling in Area CA2 during Adolescence Underlies the Emergence of PV Interneuron Plasticity and Social Memory. *Cell Reports*, 2019, 29 (5), pp.1099-1112.e4. 10.1016/j.celrep.2019.09.044 . inserm-02769625

HAL Id: inserm-02769625

<https://inserm.hal.science/inserm-02769625>

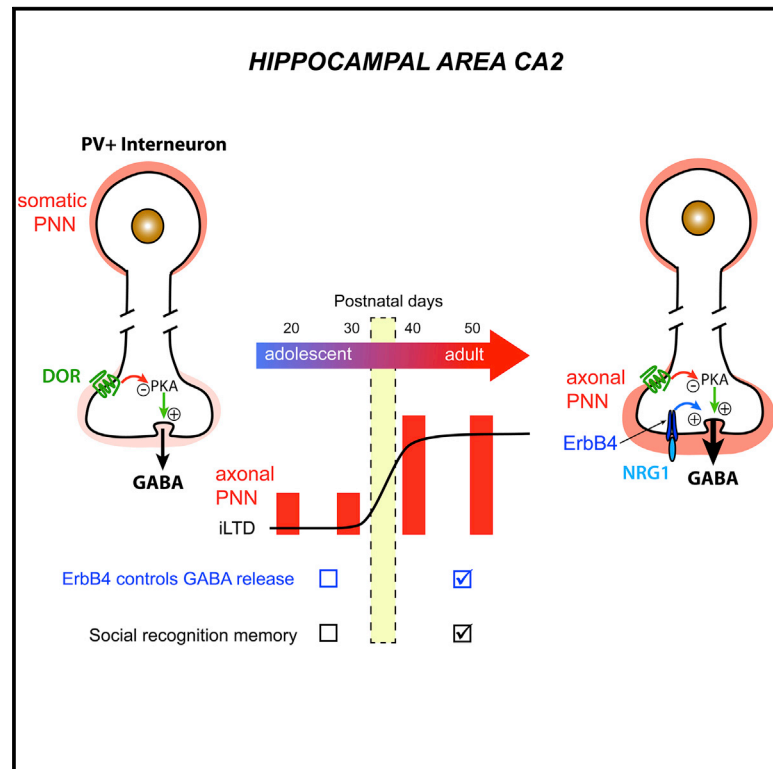
Submitted on 4 Jun 2020

HAL is a multi-disciplinary open access archive for the deposit and dissemination of scientific research documents, whether they are published or not. The documents may come from teaching and research institutions in France or abroad, or from public or private research centers.

L'archive ouverte pluridisciplinaire **HAL**, est destinée au dépôt et à la diffusion de documents scientifiques de niveau recherche, publiés ou non, émanant des établissements d'enseignement et de recherche français ou étrangers, des laboratoires publics ou privés.

Maturation of PNN and ErbB4 Signaling in Area CA2 during Adolescence Underlies the Emergence of PV Interneuron Plasticity and Social Memory

Graphical Abstract



Authors

Soledad Domínguez,
Christophe Clément Rey,
Ludivine Therreau, ..., Laure Verret,
Rebecca Ann Piskorowski,
Vivien Chevaléyre

Correspondence

vivien.chevaléyre@parisdescartes.fr

In Brief

Dominguez et al. describe the mechanisms involved in the emergence of a form of long-term plasticity at inhibitory synapses from parvalbumin-expressing interneurons in mouse hippocampal area CA2. Maturation of this plasticity potentially underlies the emergence of social memory during late adolescence.

Highlights

- Inhibitory plasticity from PV+ interneurons in area CA2 emerges at the end of adolescence
- The control of GABA release by the PNN and ErbB4 matures at the end of adolescence
- Signaling through the PNN via NRG1 and ErbB4 is required for iLTD induction
- Preventing iLTD induction in CA2 *in vivo* impairs social memory formation



Maturation of PNN and ErbB4 Signaling in Area CA2 during Adolescence Underlies the Emergence of PV Interneuron Plasticity and Social Memory

Soledad Domínguez,¹ Christophe Clément Rey,² Ludivine Therreau,^{1,4} Aurélien Fanton,¹ Dominique Massotte,³ Laure Verret,² Rebecca Ann Piskorowski,¹ and Vivien Chevaléyre^{1,5,*}

¹INSERM UMR 1266, Institute of Psychiatry and Neuroscience of Paris, Team Synaptic Plasticity and Neural Networks, 102-108 Rue de la Santé, 75014 Paris, France

²Research Center on Animal Cognition, Center for Integrative Biology, Toulouse University, CNRS, UPS, Toulouse, France

³Institut des Neurosciences Cellulaires et Intégratives, CNRS UPR 3212, 5 Rue Blaise Pascal, 67084 Strasbourg, France

⁴Inovarion, Centre de Recherche en Sciences du Vivant, 251 Rue St Jacques, 75005 Paris, France

⁵Lead Contact

*Correspondence: vivien.chevaléyre@parisdescartes.fr

<https://doi.org/10.1016/j.celrep.2019.09.044>

SUMMARY

Adolescence is a vulnerable period characterized by major cognitive changes. The mechanisms underlying the emergence of new cognitive functions are poorly understood. We find that a long-term depression of inhibitory transmission (iLTD) from parvalbumin-expressing (PV+) interneurons in the hippocampal area Cornu Ammonis 2 (CA2) is absent in young mice but emerges at the end of adolescence. We demonstrate that the maturation of both the perineuronal net (PNN) and signaling through ErbB4 is required for this plasticity. Furthermore, we demonstrate that social recognition memory displays the same age dependence as iLTD and is impaired by targeted degradation of the PNN or iLTD blockade in area CA2. Our data reveal an unusual developmental rule for plasticity at the PV+ interneuron transmission in area CA2 and indicate that this plasticity is involved in the emergence of higher cognitive function, such as social memory formation, in late adolescence.

INTRODUCTION

The hippocampus is a critical structure for learning and memory formation. Area Cornu Ammonis 2 (CA2) of the hippocampus has emerged as an important region for social memory formation (Hitti and Siegelbaum, 2014; Stevenson and Caldwell, 2014; Wersinger et al., 2002). Furthermore, this region may play an important role in the generation of hippocampal-wide network activity (Kay et al., 2016; Oliva et al., 2016). The cellular composition in area CA2 is unique in that the density of several sub-classes of interneurons, including parvalbumin-expressing (PV+) interneurons (INs), is higher than in the other hippocampal areas (Botcher et al., 2014). The inhibitory transmission from PV+ INs expresses a unique

long-term depression (iLTD) onto CA2 pyramidal neurons (PNs) that is mediated by delta opioid receptor (DOR) activation (Piskorowski and Chevaléyre, 2013).

Area CA2 is particularly vulnerable in several psychiatric diseases, including schizophrenia and dementia (Chevaléyre and Piskorowski, 2016). Specifically, the density of PV+ INs in this region has been reported to be decreased in human post-mortem studies of schizophrenic and bipolar patients (Knable et al., 2004). In a mouse model of the 22q11.2 deletion syndrome, we reported a specific decrease in PV+ IN density in area CA2, a decrease in synaptic transmission and plasticity from PV+ INs, and a deficit in social memory (Piskorowski et al., 2016). These changes in PV+ IN properties occurred at the end of adolescence, indicating that PV+ INs in area CA2 undergo developmental changes during this time period. Adolescence is a vulnerable transition period characterized by major behavioral and cognitive changes, and human imaging studies have demonstrated that the brain undergoes considerable structural development and remodeling during this period (Blakemore, 2008; Giedd et al., 1999). However, the cellular and synaptic changes that occur in the hippocampus are not understood.

The perineuronal net (PNN), a dense specialized extracellular matrix, encases PV+ IN soma and dendrites. This structure increases in density during postnatal development and often prohibits plasticity of synaptic inputs onto PV+ INs, contributing to the closure of developmental critical periods (Hensch, 2005; Horii-Hayashi et al., 2015) by regulating PV+ IN signaling (Cabungcal et al., 2013). Furthermore, it has been reported that the loss of this structure in the hippocampus is linked to schizophrenia (Berretta et al., 2015; Bitanihirwe and Woo, 2014). While rare, the PNN has been shown to also surround pyramidal cells in the cortex and hippocampus, where it surrounds CA2 PNs (Brückner et al., 2003). It has been proposed that the PNN surrounding CA2 PNs plays a role in limiting excitatory postsynaptic plasticity during early postnatal development (Carstens et al., 2016). However, the role of the PNN in controlling inhibitory plasticity during later stages of adolescence is not known.



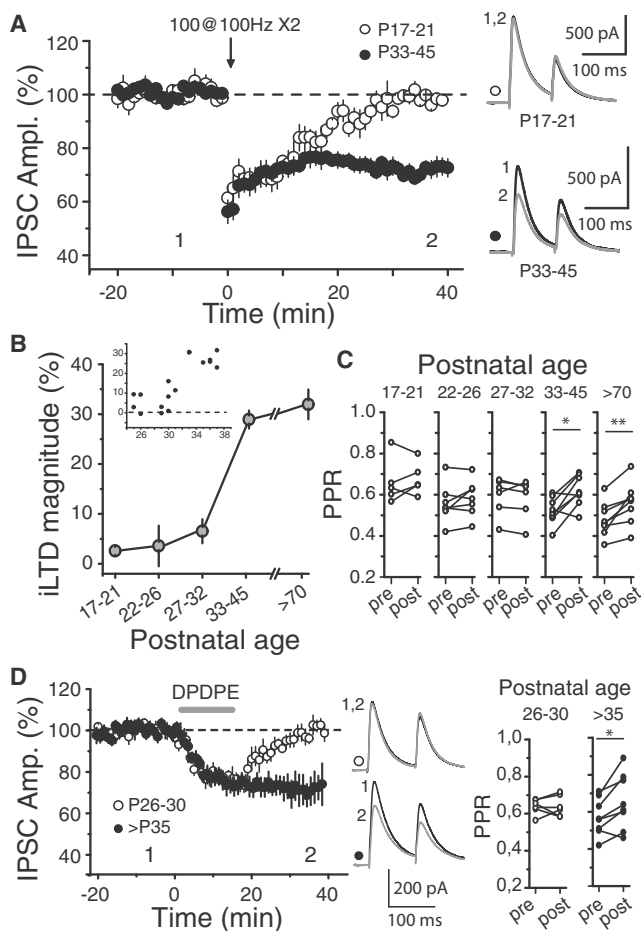


Figure 1. LTD of Inhibitory Transmission in Area CA2 Emerges at the End of Adolescence

(A) Time course of normalized IPSC amplitudes recorded in CA2 PN evoked by stimulation in the SR in the presence of α -amino-3-hydroxy-5-methyl-4-isoxazolepropionic acid (AMPA) and N-Methyl-D-aspartate (NMDA) receptor blockers. A high-frequency stimulation (HFS; 100 pulses at 100 Hz repeated twice) triggered an iLTD in slices prepared at postnatal days (P) 33–45 (filled circles, $n = 8$) but only triggered a transient depression at P17–P21 (open circles, $n = 5$). Averaged sample traces at the time points indicated are shown on the right.

(B) The summary graph of the averaged iLTD magnitude at different ages shows that the iLTD was not induced with the HFS before P27–P32 but was induced at P33–P45 and remained stable in adulthood.

(C) The HFS triggered a significant increase in the paired pulse ratio (PPR) at P33–P45 ($n = 8$, $p = 0.011$) and $>P70$ ($n = 8$, $p = 0.0058$) but not at P17–P21 ($n = 5$, $p = 0.58$), P22–P26 ($n = 7$, $p = 0.23$), or P27–P32 ($n = 6$, $p = 0.47$).

(D) Left: time course of the effect of 15-min application of 5 μ M of the selective DOR agonist (DPDPE) on normalized IPSC amplitude at P26–P30 and $>P35$. In contrast to the lasting depression-mediated DPDPE application after P35 (filled circles, $n = 8$), DPDPE triggered a transient depression at P26–P30 (open circles, $n = 6$). Center: averaged sample traces at the time indicated. Right: significant change in the PPR after the HFS at time points over P35 ($n = 8$, $p = 0.014$), but not at P26–P30 ($n = 6$, $p = 0.89$). Error bars show SEM.

In this study, we aimed to examine the cellular and molecular components that change in area CA2 during late adolescence and to determine if these changes brought about new cognitive abilities.

RESULTS

Plasticity between PV+ INs and CA2 PN Emerges at the End of Adolescence

The decrease in the density of PV+ INs and in inhibitory transmission and plasticity observed in area CA2 in a mouse model of the 22q11.2 deletion syndrome (Piskorowski et al., 2016) only occurred after the fifth postnatal week, suggesting that changes occur in PV+ IN physiology during this developmental period. Therefore, we asked whether the plasticity of PV+ INs could be developmentally regulated. We performed whole-cell voltage clamp recordings of CA2 PN to monitor inhibitory post-synaptic currents (IPSCs) evoked by stratum radiatum (SR) stimulation. We applied a high-frequency stimulation (HFS) to induce iLTD in area CA2. During postnatal days (P) 33–45, this stimulus triggered a significant iLTD of similar magnitude to what had been reported (Figure 1A; $70.9\% \pm 1.5\%$ of baseline, $n = 8$). In contrast, the same HFS did not trigger iLTD in slices prepared from animals between P17 and P21 (Figure 1A; $97.4\% \pm 1.1\%$, $n = 5$). Furthermore, we found that iLTD could not be induced at P22–P26 or at P27–P32 (Figure 1B; Table S1; P22–P26: $n = 7$, $p = 0.35$; P27–P32: $n = 6$, $p = 0.056$), then sharply increased in its magnitude between P33 and P45 and remained stable into adulthood (over P70: $n = 8$, $p = 4 \times 10^{-6}$). Consistent with the presynaptic location of the iLTD, we found that the HFS resulted in a significant increase in the paired-pulse ratio (PPR) of two consecutive IPSCs at P33–P45 and over P70 (Figure 1C; P33–P45: $p = 0.011$; $>P70$: $p = 0.0058$) but not at earlier time points (P17–P21: $p = 0.58$; P22–P26: $p = 0.23$; P27–P32: $p = 0.47$).

In adult mice, iLTD in area CA2 requires the activation of DORs (Piskorowski and Chevaleyre, 2013). Following a transient application of the selective DOR agonist [D -Pen², D -Pen⁵]enkephalin (DPDPE; 5 μ M), there was a lasting depression of IPSCs after P35 (Figure 1D; $73.5\% \pm 4.2\%$ of baseline, $n = 8$). At P26–P30, application of DPDPE induced a depression during the application, but the amplitude of the IPSCs recovered to a level similar to the initial baseline upon washout of DPDPE (Figure 1D; $98.8\% \pm 2.5\%$, $n = 6$, $p = 0.31$). Consistent with the presynaptic action of DOR activation, the DPDPE application induced a lasting increase in the PPR after P35 ($114.1\% \pm 4.1\%$, $n = 8$) but not at P26–P30 (Figure 1D; $100.6\% \pm 3.2\%$; $n = 6$). This result indicates that DORs are expressed at inhibitory synaptic terminals in young mice, but the activation of these receptors does not trigger a lasting depression of gamma-aminobutyric acid (GABA) release. Together, these data show that the iLTD in area CA2 has a late developmental maturation, with a sharp onset during the end of adolescence.

Postnatal Maturation of the PNN and Role in iLTD Induction

The DOR-mediated iLTD in area CA2 occurs at pre-synaptic terminals of PV+ INs (Piskorowski and Chevaleyre, 2013). We used immunohistochemical techniques to determine if there are any corresponding changes associated with PV+ IN density in this region during this developmental time period. Using RGS14 staining to label CA2 pyramidal cells, we examined the density of PV+ INs in areas CA1, CA2, and CA3 at four age

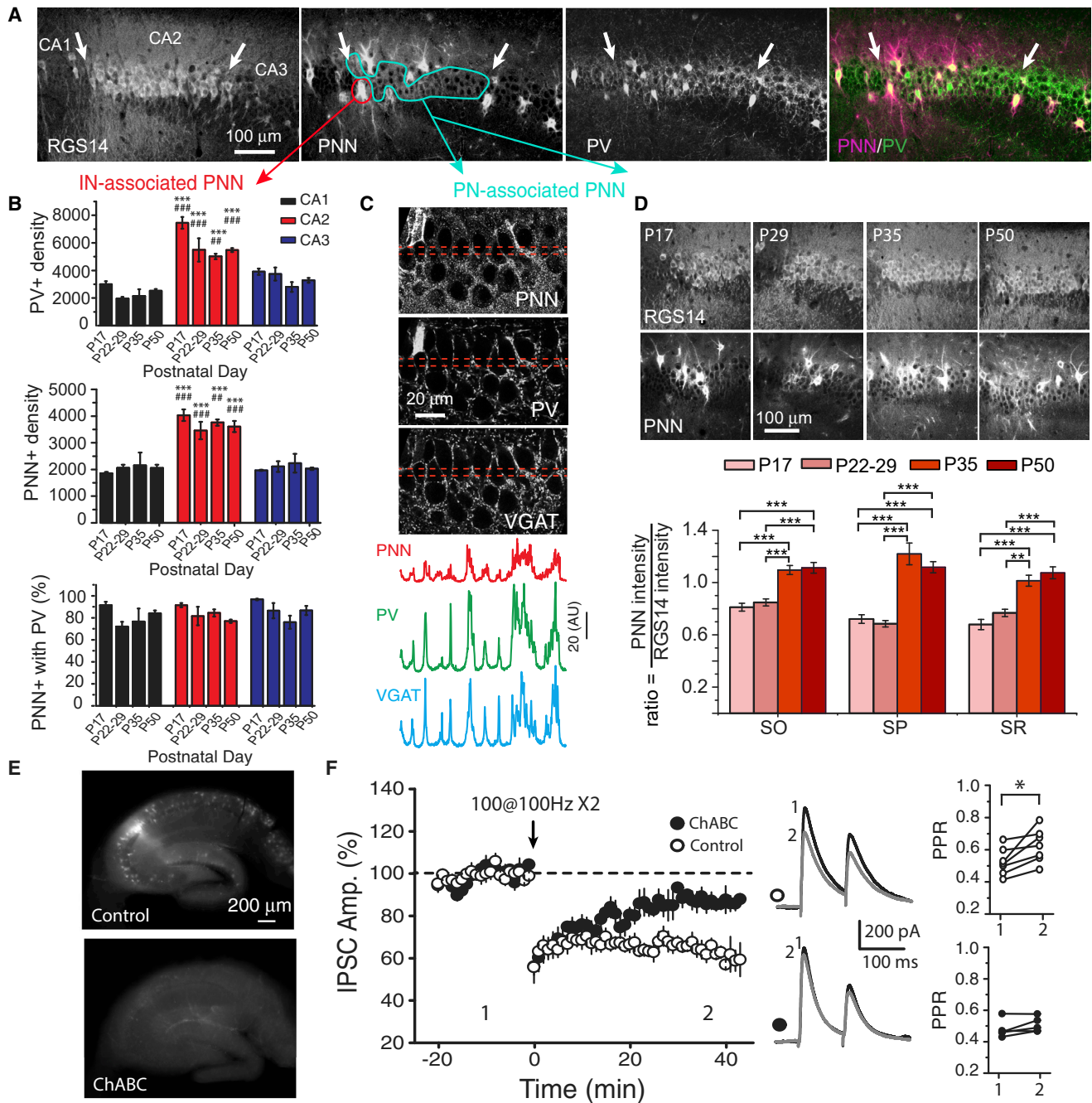


Figure 2. The Density of the PNN Associated with PV+ Synapses in Area CA2 Increases at the End of Adolescence, and Its Integrity Is Required for the iLTD

(A) Area CA2 of a P50 mouse hippocampus stained for CA2 PN marker RGS14, PNN marker Wisteria floribunda agglutinin (WFA), and parvalbumin (PV). Arrows mark the boundaries of area CA2. Far right: overlay of staining for PNN (magenta) and PV (green)

(B) Summary graph of the quantification of PV+ cells and PNN+ INs at different ages, showing that these two populations of cells are highly enriched in area CA2 at all ages studied. The percentage of co-expression between PV and the PNN show that most PNN+ cells also express PV.

(C) Top: high-magnification images of staining for PNN, PV, and VGAT. Bottom: the expression intensity profiles corresponding to the labeled region of interest in the stratum pyramidale (SP) of area CA2, showing that the PNN is in close proximity to inhibitory synapses from PV+ INs.

(D) Staining for the PNN and RGS14 in area CA2 at P17, P29, P35, and P50. Bottom graph: the quantification of the ratio of the mean PNN intensity (excluding PNN+ INs) over RGS14 intensity in area CA2 shows that a large fraction of the PNN surrounding PNs matures after P30.

(legend continued on next page)

ranges. We found that the density of PV+ cells in mice was higher in area CA2, compared to the other hippocampal areas, at all ages (Figures 2A and 2B). The PNN in area CA2 is extremely dense (Celio, 1993). We labeled the PNN with biotin-linked Wisteria floribunda agglutinin (WFA). All hippocampal CA regions contained cells that had soma and dendritic regions that were intensely labeled by WFA. The density of these cells was highest in area CA2, and the majority of the intensely labeled cells were PV+ at all ages (Figure 2B; at P50, CA2: 76.8% \pm 2.4%, CA1: 84.1% \pm 2.1%, CA3: 86.7% \pm 2.3%). These data indicate that the number of PV+ INs surrounded by the PNN does not change during the maturation of the iLTD.

Numerous studies have shown a dense PNN staining around PV+ IN soma and dendrites but also a diffuse labeling around the soma and proximal dendrites of CA2 PNs (Figures 2A and S1A; Carstens et al., 2016; Celio, 1993). The soma of PNs is mostly devoid of excitatory synapses (Megías et al., 2001), and we postulate that in area CA2, the PNN surrounding the PN soma is associated with the basket cell terminals of PV+ INs. Indeed, WFA staining was present surrounding the PV+ basket terminals encircling the soma of CA2 PNs (Figure 2C). To ensure that the PV staining around the soma of CA2 PNs corresponded to synaptic terminals and not to dendritic processes, we also co-stained for the vesicular GABA transporter (VGAT), a marker localized at inhibitory axonal terminals. We found that both PNN and PV staining profiles were very similar to the VGAT expression profile (Figure 2C). These data are consistent with the premise that the diffuse PNN staining surrounding CA2 PNs is associated with basket cell terminals from PV+ INs.

We then examined this diffuse PNN staining surrounding PN soma at different ages. We measured the mean fluorescence intensity in the different hippocampal layers of area CA2, as delimited by RGS14 staining (Figures 2D and S1), and excluded regions immediately surrounding the intensely labeled PNN+ PV+ IN soma. We found that the intensity of this diffuse WFA staining did not change between P17 and P22–P29 (Figures S1A and S1B) but significantly increased at P35 and P50. To ensure that the different PNN intensities did not result from a difference in fixation or antibody penetration at different ages, we performed two additional controls. First, we measured the intensity of the PNN staining in the same slices in area CA1. We found no change in the PNN intensity in this area (Figure S1B). Second, as the expression level of RGS14 is stable in the hippocampus during this developmental period (Evans et al., 2014), we measured the intensity of RGS14 staining at different ages and used these intensity values as an internal control. We found that the PNN density normalized to RGS14 was stable between P17 and P22–P29 but displayed a significant increase at P35 and at P50 (Figure 2D). Therefore, because the emergence of this

diffuse staining in area CA2 coincides with the emergence of the iLTD, we postulated that the PNN might play a role in iLTD induction.

We incubated hippocampal slices in Chondroitinase ABC (ChABC), thereby degrading the PNN in the entire slice, as shown by the loss of WFA staining in slices incubated with ChABC for 2 h (Figure 2E). After the ChABC incubation, the HFS induced a small iLTD (Figure 2F; 89.6% \pm 4.8%, n = 5) that was significantly smaller than the iLTD obtained in the control slices (64.2% \pm 2.6%, n = 7). After the ChABC incubation, the HFS did not trigger any significant change in the PPR, in contrast to the effect of the HFS on the PPR in the control slices (Figure 2F; in control: 119.8% \pm 5.9%; in ChABC: 106.3% \pm 3.2%). Altogether, these results indicate that the integrity of the PNN surrounding PN soma is likely associated with PV+ IN synapses and is required for iLTD induction in adult mice.

ErbB4 Is Expressed in DOR+ INs and Controls GABA Release in Area CA2

Within the PNN, there are many extracellular or transmembrane signaling molecules that can modulate neurotransmitter release. We postulate that neuregulin 1 (NRG1) and its receptor ErbB4 may play roles in regulating inhibitory transmission and plasticity in area CA2. The activation of ErbB4 by NRG1 has been reported to affect GABA release in several structures (Chen et al., 2010; Woo et al., 2007). ErbB4 is expressed by PV+ INs in the hippocampus, but it is not detected in PNs (Vullhorst et al., 2009). If ErbB4 signaling underlies the dependence on PNN integrity of the iLTD induction, it must be co-expressed by the cells that also express DORs. In the hippocampus, DORs are nearly exclusively detected in PV+ INs; however, only a fraction of PV+ INs (~40%) express DORs (Erbs et al., 2012). Similarly, ErbB4 is detected in only a fraction of PV+ INs (Bean et al., 2014). The PNN is also associated with a fraction of PV+ INs. It is unknown whether the INs that express the DOR also express ErbB4 or the PNN. To detect DORs, we used a transgenic line of knock-in mice with GFP-tagged DORs (Scherrer et al., 2006). As previously reported (Erbs et al., 2012), the vast majority of DOR-expressing neurons were located in the stratum pyramidale (SP) and stratum oriens (SO), and only a small fraction of DOR+ cells were detected in the SR. In these layers, ErbB4+ cells had a very similar localization with DOR+ cells (Figure 3; n = 5 mice). We found that the vast majority of DOR+ cells in the SO and SR co-expressed PNN and ErbB4 (Figures 3A and 3B). Similarly, a very high fraction of ErbB4+ cells in these two layers were co-labeled for the PNN and DOR (Figures 3A and 3B). Together, these data show that the majority of cells that co-express the DOR and ErbB4 are surrounded by the PNN. This finding is consistent with an implication of the PNN in iLTD induction, and it raises the question as to whether signaling through ErbB4 could be involved

(E) Incubation of acute brain slices (>P35) in chondroitinase ABC (ChABC) results in a nearly complete digestion of the PNN. Example images of two acute brain slices stained with WFA following a 2-h incubation in ACSF with vehicle (top) or 2 U/mL ChABC (bottom).

(F) Slices previously incubated in ChABC showed a much smaller iLTD following the HFS (filled circles, n = 5) compared to slices incubated with vehicle (open circles, n = 7). Averaged sample traces at the time points indicated by numbers are in the center panel. Slices pre-treated with ChABC do not undergo a significant change in PPR following HFS (bottom) as compared to controls (top). Error bars show SEM.

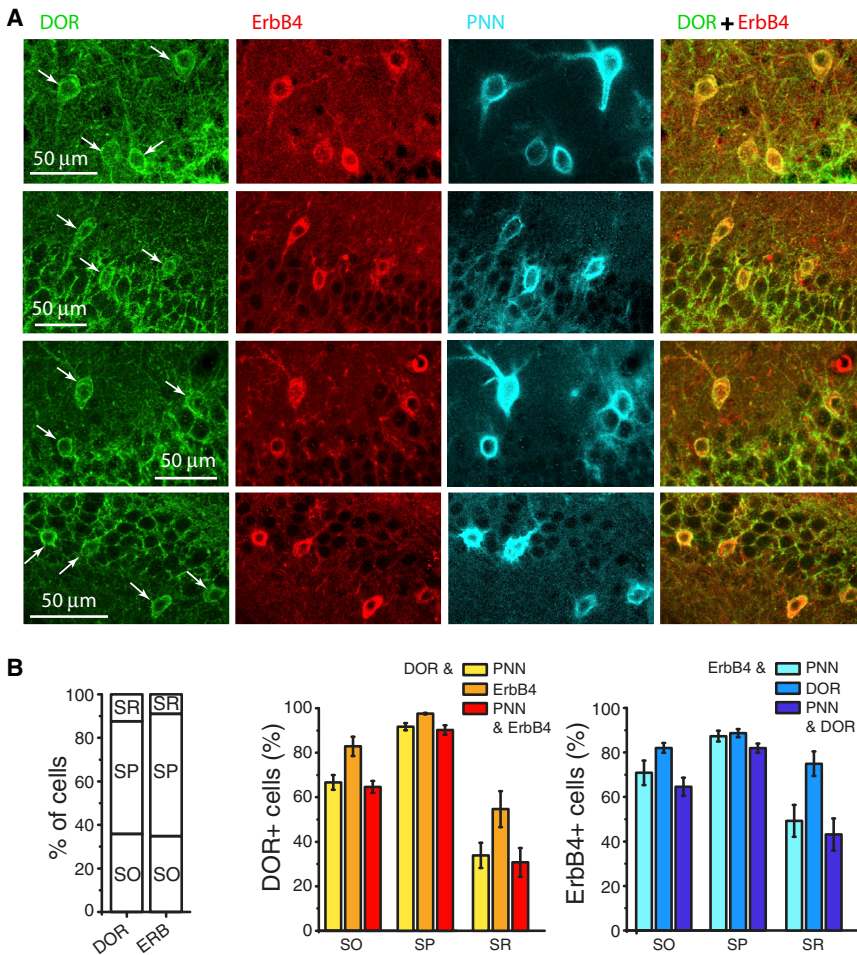


Figure 3. DOR, ErbB4, and PNN Are Colocalized in the Same Cells

(A) Triple staining against DOR-GFP (green), ErbB4 (red), and PNN (cyan) demonstrating the cellular co-localization of these markers.

(B) Left panel: summary graph of the distribution of cells that express the DOR and ErbB4 in the stratum oriens (SO), stratum pyramidale (SP), and stratum radiatum (SR). Middle: graph summarizing the percentage of DOR+ cells that were co-stained for the PNN, ErbB4, or both. Right: graph summarizing the percentage of ErbB4+ cells that were co-stained for the DOR, PNN, or both. Error bars show SEM.

0.012). However, in agreement with a lack of postsynaptic effect, the amplitude of spontaneous IPSCs was not altered (Figure 4D; $p = 0.08$). This result indicates that in area CA2 of adult mice, the release of GABA is under the control of ErbB4 and is tonically activated by endogenous NRG1. To ensure that the decrease in IPSC amplitude mediated by the ErbB4 blockade did not result from a decrease in PV+ cell excitability, and to address whether ErbB4 could affect GABA release by directly acting at the synaptic terminals, we examined how inhibiting ErbB4 altered action potential (AP)-independent miniature IPSCs (mIPSCs). Application of AG1478 induced a significant decrease in mIPSC frequency (Figures 4E and 4F; $85.1\% \pm 3.0\%$, $n = 5$; $p = 0.023$) without altering the amplitude

in the control of GABA transmission and plasticity from INs that also express the DOR.

In the cortex and area CA1, activation of ErbB4 by exogenous application of NRG1 was shown to increase GABA release (Chen et al., 2010; Woo et al., 2007). Application of the soluble active form of NRG1 (1 nM) in area CA2 did not alter evoked IPSC amplitudes or the PPR (Figure 4A; IPSC: $p = 0.7$, $n = 5$; PPR: $p = 0.66$). Further, exogenous NRG1 application also had no effect on spontaneous IPSC (sIPSC) amplitude and frequency (Figure 4B; amplitude: $n = 5$, $p = 0.14$; frequency: $p = 0.59$). This result suggests that either ErbB4 does not control GABA release in area CA2, or ErbB4 is already activated by endogenous NRG1. To explore further, we applied the ErbB4 inhibitor AG1478 to determine if basal GABA release in area CA2 is under the control of the endogenous NRG1. Following application of AG1478 (5 μ M), we observed a large decrease in evoked IPSCs onto CA2 PNs ($67.7\% \pm 4.6\%$, $n = 6$), accompanied by a significant increase in the PPR (Figure 4C; $p = 0.036$), indicating that ErbB4 activation directly affects GABA release. To confirm that ErbB4 acts presynaptically on GABA release, we also looked at the effect of the ErbB4 blocker on spontaneous IPSCs. AG1478 application induced a significant decrease in the frequency of spontaneous IPSCs (Figure 4D; $n = 6$, $p =$

$96.9\% \pm 3.8\%$, $p = 0.47$). With the change in the PPR of evoked IPSCs, these data strongly indicate that ErbB4 is located at PV+ INs' axon terminals and controls GABA release. Altogether, our data show that in contrast to the increase in inhibitory transmission mediated by the application of exogenous NRG1 in area CA1, the positive modulation of GABA release by ErbB4 in area CA2 is already maximal with endogenous NRG1.

We have previously shown that decreasing PV+ IN transmission via DOR activation strongly increases the excitatory drive between CA3 and CA2 via an increase in excitation/inhibition balance, and it results in CA2 PN AP firing (Nasrallah et al., 2015). If ErbB4 controls GABA release from the same population of INs expressing DORs, then blocking ErbB4 should increase the excitatory drive and AP firing in CA2 PNs. Application of the ErbB4 blocker AG1478 induced a large increase in field potential (fPSP) in response to the CA3 input stimulation (Figure S2A; $154.6\% \pm 11.8\%$, $n = 5$, $p = 0.009$). This increase in fPSP was abolished in the presence of GABA_R blockers, confirming that it resulted from a dis-inhibitory mechanism. Following application of AG1478, a population spike emerged in area CA2 at both 20- and 30-V stimulation intensities (Figure S2B; $p = 0.024$, $n = 4$). Thus, blocking ErbB4 led to the

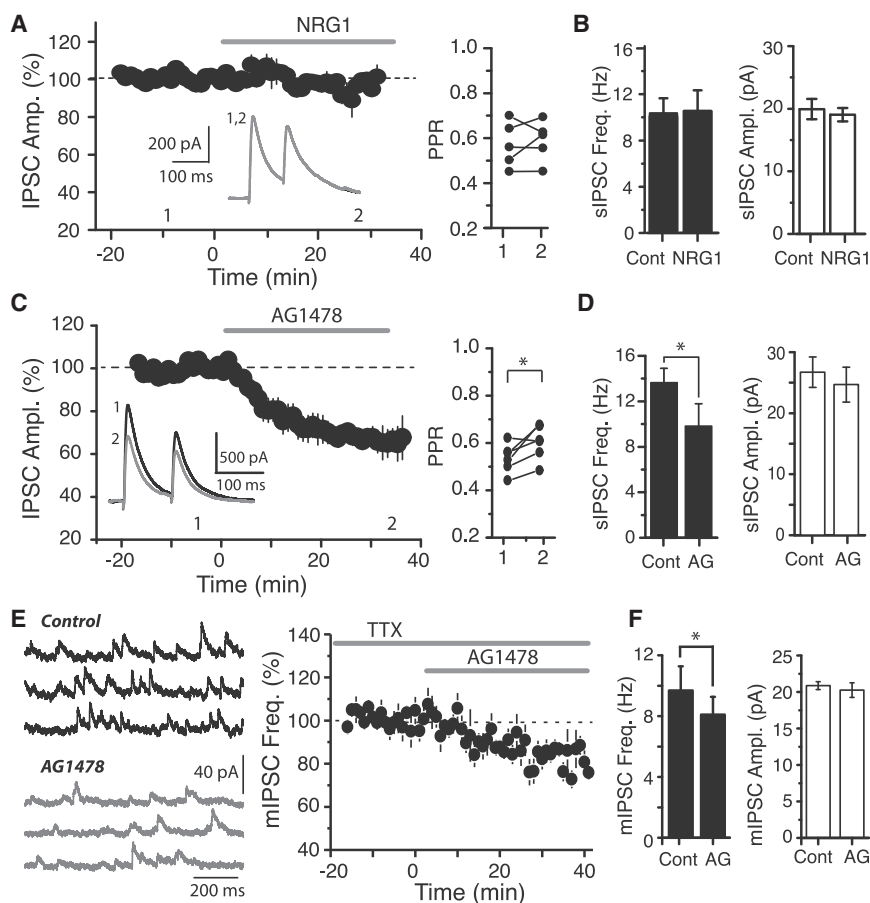


Figure 4. Signaling through ErbB4 Controls GABA Release in Area CA2 of Adult Mice

(A) Summary graph showing the lack of effect of application of the exogenous soluble form of NRG1 (1 nM) on the IPSC amplitude. Inset: averaged sample traces at the indicated time points. Right: the PPR was unchanged by application of exogenous NRG1 (n = 5).

(B) NRG1 application had no effect on the frequency (left) or amplitude (right) of sIPSCs recorded in CA2 PNs (n = 5).

(C) Summary graph of the effect of the ErbB4 inhibitor AG1478 on the amplitude of IPSCs recorded in CA2 PNs (n = 6). Inset: averaged sample traces at the time points indicated. In addition to decreasing IPSC amplitude, AG1478 (5 μ M) also triggered a significant increase in the paired pulse ratio (right panel).

(D) The ErbB4 inhibitor AG1478 induced a significant decrease in the frequency (left) but not in the amplitude (right) of spontaneous IPSCs (n = 6).

(E) Left: example traces of miniature IPSCs (mIPSCs) recorded in a CA2 PN in control conditions and after the application of AG1478. Right: summary graph of mIPSC frequency during application of AG1478 (n = 5).

(F) AG1478 induced a significant decrease in mIPSC frequency (left) but did not affect mIPSC amplitude (right) (n = 5). Error bars show SEM.

same change in the excitatory drive and AP firing in CA2 PNs as did activation of the DORs, supporting the idea that these two receptors act on the same inhibitory terminals.

Signaling through NRG1/ErbB4 Is Required for iLTD Induction

Because GABA release in area CA2 is under the control of ErbB4 activation, we tested if signaling through NRG1/ErbB4 might also be involved in the iLTD. We applied the ErbB4 inhibitor AG1478 to slices for 30 min and then applied the HFS. We found that the HFS did not evoke any iLTD in the presence of AG1478 (Figure 5A; n = 7, p = 0.637), whereas the HFS could evoke normal iLTD in interleaved control slices (n = 8, p = 0.00002). Furthermore, the PPR was not changed by the HFS in the presence of AG1478 (Figure 5A; n = 7, p = 0.4) but significantly increased in the control slices (Figure 5A; n = 8; p = 0.0087).

To ensure that the impaired iLTD induction following the blockade of ErbB4 is not due to reduced enkephalin release, we directly activated DORs by DPDPE application. In the presence of AG1478, DPDPE did not trigger iLTD or any lasting change in the PPR (Figure 5B; IPSC: $97.9\% \pm 1.7\%$, n = 6, p = 0.11; PPR: $98.1\% \pm 5.2\%$, n = 6, p = 0.78). These data are consistent with the fact that inhibition of ErbB4 decreases

GABA release from the same neurons that express the DOR; therefore, blocking ErbB4 occluded a further depression by DOR activation. We also tested whether NRG1 could affect the iLTD. In the presence of the soluble form of NRG1, the HFS was ineffective at inducing the iLTD (Figure 5A; $96.6\% \pm 1.5\%$ of baseline, n = 5, p = 0.087) and produced no significant change in the PPR (Figure 5A; n = 5, p = 0.091). Therefore, even though exogenous NRG1 application had no effect on the basal transmission because of the endogenous activation of ErbB4 (see Figure 4), the presence of exogenous NRG1 prevented iLTD induction. One possible explanation is that the endogenous activation of ErbB4 is decreased following iLTD induction. Indeed, neuronal activity regulates numerous enzymes in the extracellular matrix (Dzwonek et al., 2004). Therefore, it is possible that a decrease in NRG1 availability or in ErbB4 signaling occurs following the tetanus. To test this, we applied NRG1 5 min after the tetanus. We found that following the NRG1 application, the depression in IPSCs was not maintained, and GABA transmission returned to a value that was significantly different from the depression observed in interleaved control slices (Figure 5C; n = 6 and 6, p = 0.00032). In addition, the change in the PPR at the end of the experiment was also significantly smaller after the NRG1 application (Figure 5C; n = 6 and 6, p = 0.026). These data are consistent with the idea that part of the NRG1-ErbB4 action on GABA release was downregulated after the HFS, and exogenous activation of ErbB4 prevented the maintenance of the iLTD.

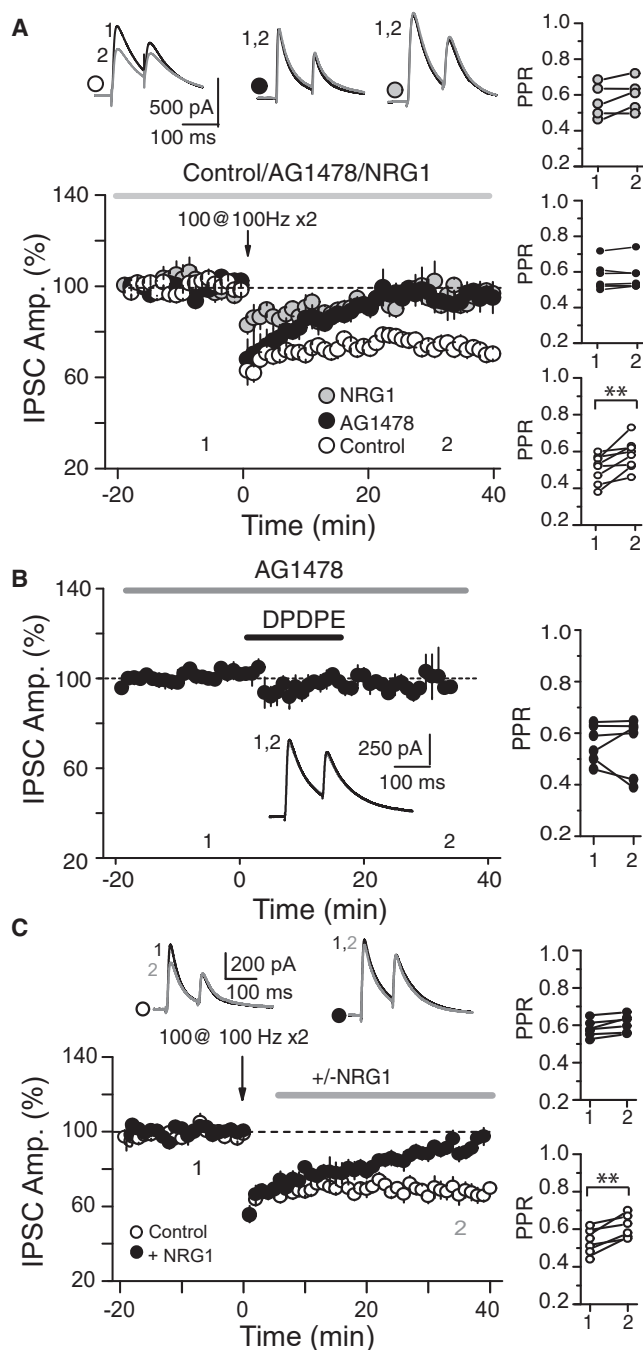


Figure 5. NRG1/ErbB4 Signaling Is Required for DOR-Mediated Plasticity

(A) Incubation of slices in AG1478 (black circles, $n = 7$) or NRG1 (gray circles, $n = 5$), followed by continuous application of these drugs, prevented iLTD induction by the HFS. The iLTD was normal in interleaved control slices (white circles, $n = 8$). Top: averaged sample traces at the time point indicated. The increase in the PPR observed in control slices was also prevented by the presence of AG1478 or NRG1 (right).

(B) Blockade of ErbB4 by AG1478 also prevented the effect of the DOR agonist application on the IPSCs amplitude and on the PPR ($n = 6$). Inset: averaged sample traces at the time point indicated by numbers.

The Effect of NRG1/ErbB4 Signaling on GABA Release Is Age Dependent

Both ErbB4 and NRG1 are expressed early during development and control several processes such as migration and maturation of PV+ cells (Mei and Xiong, 2008). However, it is unknown whether ErbB4 can control GABA transmission in young animals and if this may underlie the lack of iLTD in young mice. To test this, we examined the effect of AG1478 on inhibitory transmission in P22–P27 mice. In contrast to what we observed in the adult mice, application of AG1478 had no effect on the evoked IPSC amplitude (Figure S3A; $n = 6$, $p = 0.13$) or on the PPR ($n = 6$, $p = 0.71$). In addition, the AG1478 application did not change the frequency or amplitude of sIPSCs (Figure S3B; frequency: $p = 0.66$; amplitude: $p = 0.84$, $n = 6$). We then asked if the lack of action of the ErbB4 blocker might result from a lack of endogenous activation by NRG1 or from a lack of control of GABA release by ErbB4. We found that exogenous NRG1 (1 nM) application had no effect on the evoked IPSC amplitude (Figure S3C; $n = 5$, $p = 0.29$) or on the PPR ($p = 0.062$) in P22–P27 mice. Furthermore, NRG1 also did not change the frequency or amplitude of sIPSCs at this age (Figure S3D; frequency: $p = 0.61$; amplitude: $p = 0.34$, $n = 5$). We also tested lower (0.1 nM) and higher (10 nM) concentrations of NRG1 and still found no effect on the evoked IPSC amplitude or the PPR (Figures S3E and S3F). Therefore, these data show that the modulation of GABA release by ErbB4 is age dependent. In adult mice, GABA transmission is positively modulated by the endogenous activation of ErbB4. In young mice, endo- or exogenous NRG1 had no action on GABA transmission, suggesting the ErbB4 is not expressed at the synapse and/or is not coupled to GABA release.

DOR and ErbB4 Engage Different Signaling Pathways

Our data indicate that both DORs and ErbB4 are required for iLTD induction. Therefore, we wondered whether these two receptors might use the same signaling pathway. DORs are known to activate G-proteins negatively coupled to adenylyl cyclase (Quock et al., 1999). Thus, we wondered whether the cyclic AMP (cAMP)/protein kinase A (PKA) pathway might be involved in iLTD. We incubated slices for 30 min in the PKA blocker PKI 14–22 amide (PKI; 1 μ M) and continuously applied it throughout the plasticity measurement. Following the PKA block, the HFS did not trigger any significant iLTD (Figure 6A; $n = 5$, $p = 0.052$) or changes in the PPR ($p = 0.59$). In contrast, we observed in interleaved control experiments a significant depression of IPSCs ($n = 5$, $p = 0.0004$) and a change in PPR ($p = 0.028$) after the HFS. To ensure that the lack of iLTD did not result from a lack of enkephalin release, we also tested the effect of the DOR agonist DPDPE in the presence of PKI. DPDPE did not induce any depression of the IPSC amplitudes with the PKA blocked (Figure 6B; $p = 0.79$, $n = 5$) and also did not affect the PPR ($p = 0.18$). These data confirm that the PKA is required for the depression of GABA release mediated by

(C) Application of NRG1 5 min after tetanus (black circles, $n = 7$) reverses the IPSC depression, and an increase in the PPR is observed in control slices (white circles, $n = 6$). Error bars show SEM.

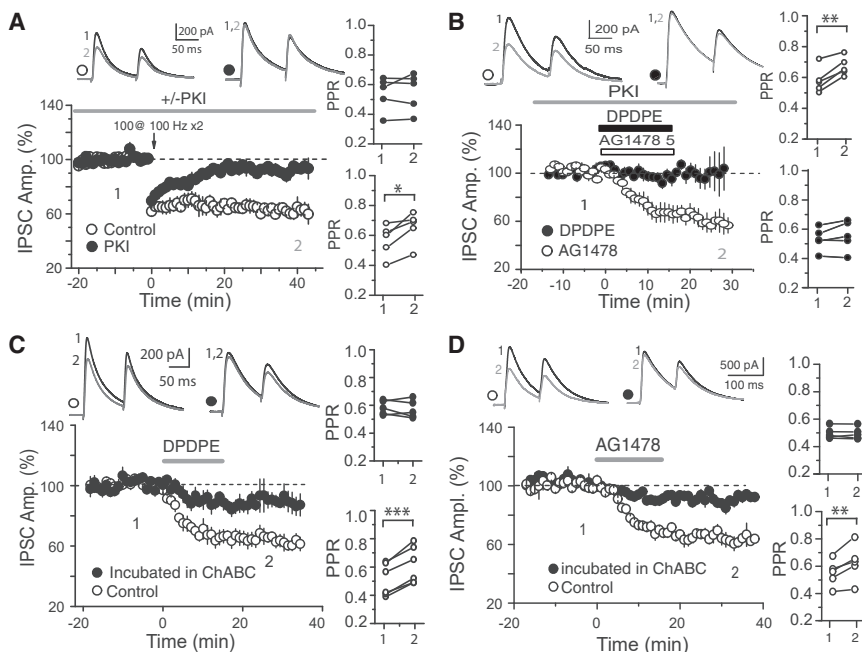


Figure 6. DOR and ErbB4 Engage Different Signaling Pathways, but Their Action on GABA Release Is Dependent on the PNN Integrity

(A) Blockade of PKA with PKI 14–22 amide completely abolished the iLTD induction and change in the PPR induced by a tetanus (black circles, $n = 5$). Slices were incubated 30 min in PKI and recorded in the continuous presence of PKI.

(B) In the presence of PKI, DOR activation by DPDPE had no effect on GABA transmission (black circles, $n = 5$). In contrast, the PKA blockade did not affect the depression of IPSCs induced by the ErbB4 blocker AG1478 (white circles, $n = 5$).

(C) Application of DPDPE resulted in a significantly smaller depression of IPSCs in slices previously incubated in ChABC (filled circles, $n = 5$) as compared to control slices (open circles, $n = 6$). Top: averaged sample traces at the time points indicated by numbers. Right: prior treatment by ChABC prevents a significant change in the PPR following DPDPE application.

(D) In slices previously incubated in ChABC (black circles, $n = 5$), blockade of ErbB4 by AG1478 resulted in a significantly smaller depression of

IPSCs compared to control slices (white circles, $n = 5$). The change in the PPR was also prevented by previous incubation in ChABC. Top: averaged sample traces at the time points indicated. Error bars show SEM.

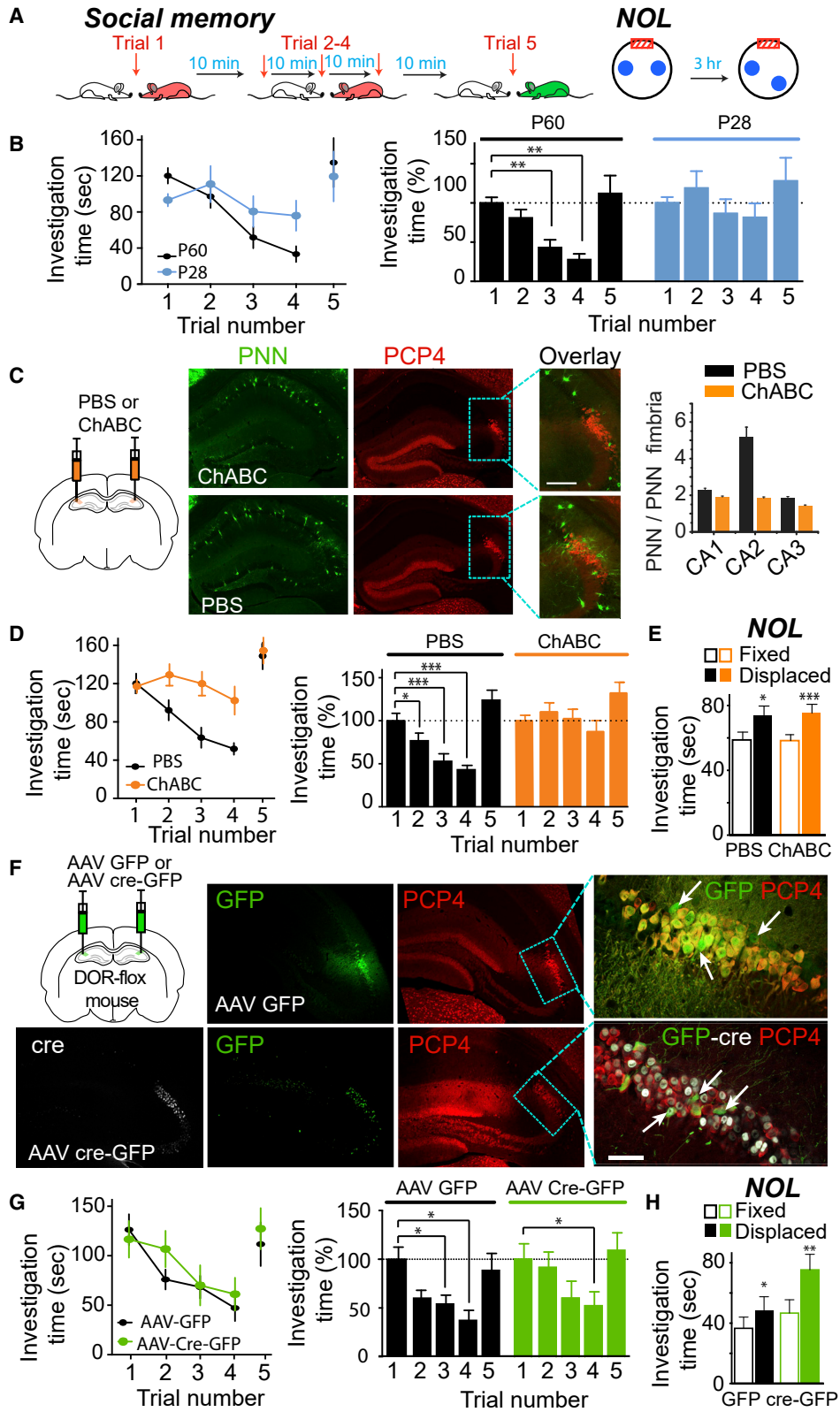
the DOR. Next, we tested whether ErbB4 action on GABA release also involves the PKA. We found that in presence of PKI, AG1478 induced a large depression of the IPSC amplitudes (Figure 6B; $p = 0.0012$, $n = 5$) and an increase in the PPR ($p = 0.005$). Therefore, these data show that the DOR and ErbB4 use different signaling pathways to control GABA release in area CA2.

Next, we asked whether the PNN plays a role in the DOR- and ErbB4-mediated control of GABA release. First, we tested the consequence of PNN degradation on the decrease in GABA release mediated by the DOR activation. In slices incubated with ChABC, DPDPE application had a smaller effect on synaptic transmission (Figure 6C; $n = 5$) and the PPR, compared to slices incubated in vehicle ($n = 6$, IPSC: $p = 0.003$; PPR: $p = 0.00011$). These data suggest that the PNN is required for the modulation of GABA release by the DOR activation. We also tested the effect of the PNN degradation in area CA1 on the DOR action. In area CA1, the PNN is not detected at basket cell terminals, and activation of the DOR resulted in a transient decrease in inhibitory transmission from PV+ INs (Piskorowski and Chevaleyre, 2013). Application of DPDPE resulted in a transient depression of IPSCs that returned to baseline for both control and ChABC-treated slices (Figure S4; $p = 0.92$). Furthermore, no lasting change was detected in the PPR for both conditions (control: $n = 5$, $p = 0.59$; ChABC: $n = 5$, $p = 0.20$). The transient depression of the IPSC amplitude at the end of DPDPE application was identical in both conditions ($p = 0.95$). Therefore, these data show that degradation of the PNN in area CA1, which primarily surrounds soma and dendrites of INs, did not affect the action of the DOR activation on GABA transmission. We then tested the effect of PNN degrada-

tion on the control of GABA release by ErbB4. We found that AG1478 induced a very small depression of IPSCs in ChABC-treated slices (Figure 6D; $n = 5$), compared to controls ($n = 5$). AG1478 also had very little effect on the PPR in ChABC-treated slices (Figure 6D; $n = 5$), compared to controls ($n = 5$). Therefore, these data indicate that when the PNN is degraded, the positive action of ErbB4 on GABA release is lost, suggesting that PNN integrity is required for the basal activation of ErbB4 by endogenous NRG1.

DOR-Mediated iLTD in CA2 Is Involved in Social Memory Formation

The late emergence of the iLTD suggests that this plasticity may be involved in higher cognitive processes rather than synapse and network establishment. If DOR-mediated iLTD in area CA2 plays a role in social memory formation, one could make the following two predictions. First, the ability of a mouse to form social memories should emerge during development at the same time as the iLTD. Second, disruption of the iLTD in adult mice should also disrupt performance in a social memory task. To test these predictions, we first examined the ability of a mouse to form social memories before and after the onset of iLTD with the five-trial social memory test (Kogan et al., 2000; Figure 7A). In adult control mice, the interaction time was significantly reduced in trials 3 and 4 with the same familiar mouse (Figure 7B; $n = 8$). When a novel mouse was introduced in trial 5, the subject mouse displayed an expected rebound of interaction time. In 28-day-old mice, there was no significant decrease in the interaction time in trials 2–4, compared to trial 1 (Figure 7B; $n = 10$). These data indicate that before the emergence of the DOR-mediated iLTD in area CA2, juvenile



(legend on next page)

mice show a performance in this task that is consistent with reduced social memory.

Next, we tested whether disrupting the iLTD specifically in area CA2 would also affect social memory in adult mice. We used two different strategies to test this hypothesis. First, because iLTD is dependent on the PNN integrity, we performed targeted bilateral stereotaxic injections into area CA2 to deliver either a control saline solution or a ChABC solution. Then, 7 days following the injection, we performed the same social memory test on the two groups of animals. Behavioral data were only used from animals that had injection sites properly targeted to area CA2. After the targeted injection of 0.1 μ l of ChABC in area CA2, the intensity of the PNN staining was slightly reduced in areas CA1 and CA3 but displayed a much larger decrease in area CA2 (Figure 7C). We found that the initial interaction time between the subject mouse and a novel mouse did not differ between ChABC- and vehicle-injected mice, suggesting that sociability is not affected by reducing the PNN in area CA2. In mice injected with saline, a significant decrease in the interaction time was observed during trial 2 (Figure 7D; $n = 10$), and a further decrease was observed in trials 3 and 4. For mice injected with ChABC, no significant decrease in interaction time between the subject mouse and the familiar mouse was observed, even during trial 4 (Figure 7D; $n = 12$). Therefore, these results indicate that digestion of the PNN in area CA2 is sufficient to prevent social memory formation.

Because we cannot exclude that a small-level PNN degradation in areas CA1 or CA3 could also contribute to the behavior, we performed two hippocampal-dependent but CA2-independent tasks after ChABC injection in area CA2. First, we monitored the distance traveled in an open field and the time spent in the center of the arena. We found that the total distance was not different between saline- and ChABC-injected mice (PBS: $n = 6$; ChABC: $n = 8$, $p = 0.62$). Similarly, the time spent in the center was not different between saline- and ChABC-injected mice (PBS: $n = 6$; ChABC: $n = 8$, $p = 0.081$). These data suggest that both general locomotor activity and anxiety are not altered following PNN degradation in area CA2. Next, we performed a novel object location task. During acquisition of the task, both saline- and ChABC-injected mice spent the same amount of time exploring the two different objects (PBS: $n = 6$, $p = 0.26$;

ChABC: $n = 8$, $p = 0.28$). During the test, both PBS- and ChABC-injected mice spent significantly more time exploring the displaced object compared to the fixed object (Figure 7E; PBS: $p = 0.03$; ChABC: $p = 0.00079$). Therefore, this result suggests that the impairment in social memory formation after ChABC injection was the result of the PNN digestion in area CA2 and not in areas CA1 or CA3.

We have shown that PNN integrity in area CA2 is required for iLTD induction. However, we employed a second strategy to target area CA2 in order to rule out alterations of DOR-mediated plasticity in area CA3, as there is a high expression of DORs in inhibitory neurons in area CA3 (Erbs et al., 2012), and CA3 has recently been implicated in the encoding phase of social memory (Chiang et al., 2018). In contrast to a previous study (Leroy et al., 2017), we found that DPDPE application induced a large and significant decrease in inhibitory transmission in CA3 PNs (Figure S5; $n = 5$, $p = 0.005$), along with an increase in the PPR ($n = 5$, $p = 0.02$), consistent with a presynaptic action of the DOR on GABA release. Our second strategy took advantage of the binding of adeno-associated viruses (AAVs) to glycan regions of host cell receptors (Mietzsch et al., 2014). The PNN present in area CA2 is particularly rich in proteoglycans and sialic acids (Brückner et al., 2003), and we harnessed this aspect of the extracellular matrix to knockout DOR receptors selectively in area CA2. We used a DOR-flox mouse line (Orpd1^{flox}) and performed a very small volume targeted injection to area CA2 of an AAV serotype 5 virus expressing GFP-tagged Cre recombinase (AAV5-cre-GFP) or control virus expressing GFP (AAV5-GFP). Then, 6 weeks after viral injection, we tested the performances of the social memory and novel object location tasks. Following the behavioral testing, the specificity of the viral infection was confirmed post hoc (Figure 7F). Behavioral data were only used from animals that had injections properly targeted to area CA2. The viruses led to GFP expression in PCP4-expressing PNs as well as putative INs in area CA2, as these cells were smaller in size and PCP4 negative, yet located within the PCP4+ region (Figure 7F).

Mice injected with the control virus displayed a learning curve similar to that of the control mice, with a large decrease in interaction time observed during trials 2–4 and a rebound of interaction during trial 5 (Figure 7G; $n = 7$). In mice injected

Figure 7. Social Memory Matures in Parallel to the iLTD and Requires the PNN Integrity in CA2

(A) Left: illustration of the experimental protocol used to test social memory formation. Right: illustration of the experimental protocol used to perform novel object location task (NOL).

(B) In P60 mice, investigation time decreased during successive exposures and was significantly lower in trials 3 and 4 ($n = 8$) compared to trial 1. In P28 mice, no significant decrease in interaction time was observed in trials 2–4 ($n = 10$). Right panel shows the normalized investigation time at P60 and P28.

(C) Staining for the PNN (green) and for the CA2 marker PCP4 (red) in mice injected with ChABC or saline solution (PBS). Right: a large decrease in the PNN staining in area CA2 is observed in mice injected with ChABC. Scale bar: 100 μ m.

(D) Mice injected with PBS show a normal decrease in interaction time in trials 2–4 ($n = 10$). The interaction time did not decrease on trial 2–5 as compared to trial 1 for mice injected with ChABC ($n = 12$). The normalized values for the interaction time show that a significant decrease in interaction was observed in PBS-injected mice on trials 2–4, whereas no significant change was observed in mice injected with ChABC.

(E) Both PBS- and ChABC-injected mice display a preference for the displaced object in the NOL task.

(F) Staining for GFP (green), PCP4 (red), and Cre (white) in DOR-flox mice injected with AAV GFP or AAV cre-GFP in area CA2. Higher magnifications are shown on the right. Arrows show GFP-positive, PCP4-negative neurons (putative INs). Note the nuclear localization of the cre-GFP signals in AAV cre-GFP-injected mice. Scale bar: 50 μ m.

(G) Mice injected with AAV GFP show a large decrease in interaction time in trial 2 and a significant decrease in trials 3 and 4 ($n = 7$). In contrast, mice injected with AAV cre-GFP ($n = 8$) only show a significant decrease in interaction time in trial 4, indicating that acquisition of social memory is delayed.

(H) Both AAV GFP- and AAV cre-GFP-injected mice display a preference for the displaced object in the NOL task. Error bars show SEM.

with AAV-cre-GFP, a significant decrease in interaction time between the subject and the familiar mouse was observed only during trial 4 (Figure 7G; $n = 9$). To ensure that CA2-independent but hippocampal-dependent tasks were not affected by the viral injection, we also looked at the open field and the novel object location tasks. In the open field task, both AAV-cre-GFP and AAV-GFP mice traveled the same distance in the arena (AAV-GFP: $n = 7$; AAV-cre-GFP: $n = 9$, $p = 0.221$) and spent the same amount of time in the center (AAV-GFP: $n = 7$; AAV-cre-GFP: $n = 9$, $p = 0.397$). In the novel object location task, both AAV-cre-GFP and AAV-GFP mice spent similar amounts of time exploring the two novel objects (AAV-GFP: $n = 7$, $p = 0.20$; AAV-cre-GFP: $n = 9$, $p = 0.82$). Both mice also spent more time exploring the displaced object (Figure 7H; AAV-GFP: $p = 0.026$; AAV-cre-GFP: $p = 0.006$). Altogether, these data show that preventing DOR-mediated plasticity in area CA2 did not alter general locomotor activity and anxiety. However, the lack of the DOR in area CA2 delays the acquisition of social recognition memory.

DISCUSSION

In this study, we show that the DOR-mediated plasticity of GABA release from PV+ INs in area CA2 has a reversed developmental profile compared to many forms of plasticity. Its emergence at the end of adolescence coincides with the maturation of the PNN and ErbB4 signaling at PV+ IN synapses, and both the PNN and ErbB4 are required for the induction of the plasticity. Furthermore, we provide evidence that DOR-mediated plasticity plays a facilitatory role in social memory formation and emergence of this memory at the end of adolescence.

Model for DOR-Mediated iLTD at PV+ IN to PN Synapses

We propose the following model for iLTD induction (Figure S6). In juvenile mice, the action of DOR activation is transient, and transmission recovers to basal levels upon washout of the agonist or 10–15 min after tetanus; ErbB4 is either not expressed at the synapse, or it is expressed but its activation is not linked to GABA release. In adult mice, PV+ INs that express DORs also express ErbB4; ErbB4 activation controls GABA release and in basal conditions is activated by endogenous NRG1. After the HFS, GABA release is reduced through the DOR activation. The tetanus also leads to a loss of ErbB4 activation, either through a direct link between the DOR and ErbB4 or through a change in the availability of soluble NRG1. The loss of positive action of ErbB4 can then maintain the depression of GABA release, thus leading to iLTD. Reactivation of ErbB4 with exogenous NRG1 just after the tetanus restores GABA transmission and prevents iLTD. The PNN appears to play a critical role in iLTD induction by allowing ErbB4 to be activated by NRG1. After PNN degradation, blockade of ErbB4 has no effect on GABA transmission, and the iLTD cannot be induced and is likely occluded. Other manipulations that decrease GABA release from PV+ INs, such as the DOR agonist application or direct ErbB4 blockade, also occlude the iLTD. Therefore, these data highlight a critical role of PNN maturation around PV+ IN synapses in the emergence of the iLTD, likely by allowing ErbB4 action on GABA release.

PNN Maturation during Late Adolescence Controls the Emergence of Plasticity at PV+ Synapses in Area CA2

Several studies have reported an increase in the PNN staining during postnatal hippocampal development (Carstens et al., 2016; Horii-Hayashi et al., 2015; Yamada and Jinno, 2013). Here, we report an increase in the PNN likely associated with inhibitory terminals on CA2 PNs during late adolescence. It was initially proposed that the PNN around CA2 PN soma could be associated with inhibitory synapses from basket cells (Celio, 1993). More recently, it was proposed that the PNN around CA2 PNs serves to regulate excitatory transmission and plasticity during early postnatal development (Carstens et al., 2016). The soma of hippocampal PNs is virtually devoid of excitatory synapses and is instead surrounded by inhibitory terminals from basket cells (Megias et al., 2001). In area CA2, the fraction of basket cell terminals from PV+ INs around the soma of PNs is much higher than in areas CA1 or CA3 (Ribak et al., 1993). Therefore, we postulate that the PNN around the soma of CA2 PNs is associated with inhibitory synapses from PV+ cells and, thus, would be able to influence GABA release. In agreement with this idea, we found that degradation of the PNN prevents DOR-mediated iLTD induction, a plasticity known to occur at pre-synaptic terminals of PV+ INs (Piskorowski and Chevaleyre, 2013). DOR receptors are expressed at synaptic terminals of PV+ INs (Rezaei et al., 2012), and we show that PNN degradation strongly reduces the effect of their activation on GABA release. Finally, we found that endogenous activation of ErbB4 is required for iLTD induction and controls both the amplitude of evoked IPSCs and the frequency of mIPSCs. Therefore, these data demonstrate that the PNN-associated signaling through ErbB4 is involved in controlling the release of GABA from PV+ IN terminals.

Inhibitory transmission from PV+ INs onto CA2 PNs displays a long-term depression mediated by DOR activation (Piskorowski and Chevaleyre, 2013). We show that this plasticity is not expressed in juvenile mice but shows a steep increase after P30. These data are in sharp contrast to many forms of plasticity that are prominent during postnatal development but are considered constrained by maturation of the PNN at the end of adolescence. For instance, maturation of the PNN has been shown to be a break for plasticity in the cortex and to control the end of the critical period (Hensch, 2005). Our data suggest that components of the PNN can also have a permissive role for synaptic plasticity by supporting the iLTD induction in area CA2. Several results strongly suggest that maturation of the signaling through the PNN is required for the emergence of iLTD: (1) the intensity of the PNN staining associated with inhibitory basket terminals in area CA2 shows a large increase in intensity after P30; (2) PV+ cells that express the PNN-associated ErbB4 also express DORs; (3) disrupting PNN integrity in adults also disrupts iLTD induction; and (4) signaling through ErbB4/NGR1 controls the probability of GABA release in adults but not in young mice and is required for iLTD induction. Together, these data show that in contrast to many forms of plasticity that are constrained by maturation of the PNN at the end of adolescence, signaling within the PNN can be permissive for the emergence of new plasticity and potentially higher cognitive functions.

The Role of Plasticity at PV+ Synapses in Area CA2 in Social Memory Formation

Area CA2 plays a critical role in social memory formation. This form of memory is impaired when tetanus toxin is expressed in CA2 PNs (Hitti and Siegelbaum, 2014), indicating that transmission from CA2 PNs is required. In agreement, social memory is also impaired in a mouse model of the 22q11.2 deletion syndrome, where excitability of CA2 PNs is strongly reduced (Piskorowski et al., 2016). Normally, CA3 inputs are unable to drive AP firing in CA2 PNs because of the large feed-forward inhibition between areas CA3 and CA2 (Chevalleyre and Siegelbaum, 2010; Kohara et al., 2014; Piskorowski and Chevalleyre, 2013). However, following iLTD induction in area CA2, CA3 inputs are able to drive AP firing in CA2 PNs (Nasrallah et al., 2015). Because excitatory CA3-CA2 inputs do not express activity-dependent long-term-potential (LTP) (Zhao et al., 2007), it is likely that plasticity at inhibitory synapses represents a primary means of modulating the excitability of CA2 PNs. Our data provide evidence that iLTD may play an active role in social memory formation. (1) Social memory matures at the same time as the iLTD. The lack of social memory in juvenile mice is not just a generalized inability to learn because mice at this age or even younger have been shown to learn diverse tasks such as spatial memory (Ainge and Langston, 2012) or contextual fear conditioning (Pattwell et al., 2013). These tasks are dependent on the hippocampus, but they are independent of area CA2 (Hitti and Siegelbaum, 2014). (2) We show that localized degradation of the PNN in CA2, a manipulation that impairs iLTD induction, also impairs social memory formation. (3) We provide evidence that selective removal of DORs in area CA2 also affects social memory formation. In contrast to PNN degradation, this manipulation did not fully block social memory. Several explanations can be put forward to explain this difference. In particular, PNN degradation can alter the excitability of PV+ INs (Bozzelli et al., 2018; Hayani et al., 2018) in addition to preventing iLTD induction. Therefore, it is likely that PNN degradation will result in a stronger impairment of PV+ IN physiology than just selective knockout of DORs. The reduced social memory that we observed after the DOR removal is consistent with the decrease observed after the DOR antagonist injection in CA2/CA3 (Leroy et al., 2017). However, using a five-trial social memory test instead of two trials only, we were able to show that the interaction times during the second and third trials were altered, but the interaction time was normal during the fourth trial. Therefore, these data indicate that social learning is slower in mice lacking a DOR in area CA2, but these mice are still able to form normal social memory.

The data presented here are not only relevant for understanding the mechanisms involved in the emergence of new cognitive functions at the end of adolescence, but they also provide valuable insights on potentially relevant alterations occurring during pathologies. Multiple post-mortem studies have demonstrated that area CA2 is particularly susceptible during psychiatric diseases and neurodegenerative disorders (Chevalleyre and Piskorowski, 2016). Furthermore, several studies have reported that the PNN and ErbB4 signaling are altered during schizophrenia and Alzheimer's disease (Berretta et al., 2015; Iwakura and Nawa, 2013; Soleman et al., 2013).

The PNN contains neurotrophic factors and is neuroprotective for PV+ INs against oxidative stress (Cabungcal et al., 2013). Therefore, a deficit in signaling through the PNN may underlie the decrease in PV+ IN density observed during these pathologies. In area CA2, we show that the PNN is also likely located between the axon terminal of PV+ INs and the soma of PNs, where it can control synaptic transmission and the plasticity of GABA release. A large fraction of this PNN matures at the end of adolescence in parallel to the control of GABA release mediated by endogenous ErbB4 activation. Therefore, it is possible that an impaired signaling within the PNN may underlie the decrease in inhibitory transmission and plasticity that we observed in a mouse model of the 22q11.2 deletion syndrome, the highest genetic risk factor for developing schizophrenia in humans (Karayiorgou et al., 2010; Piskorowski et al., 2016). In agreement with this, both NRG1 and ErbB4 have been linked to schizophrenia (Buonanno, 2010), and removing ErbB4 from fast-spiking INs is sufficient to cause a schizophrenia-like phenotype (Del Pino et al., 2013). Furthermore, it has been proposed that signaling through NRG1 and ErbB3/4 is involved in social memory (Moy et al., 2009). Our data suggest that this effect could be mediated through plasticity at inhibitory synapses in area CA2, and this pathway might be altered during schizophrenia.

Altogether, our data show that the maturation of the PNN and of ErbB4 signaling is a prerequisite for the emergence of plasticity at PV+ IN synapses in area CA2. Furthermore, the data also provide evidence that the late maturation of inhibitory plasticity in area CA2 might be involved in emergence of higher cognitive processes such as social memory formation.

STAR★METHODS

Detailed methods are provided in the online version of this paper and include the following:

- KEY RESOURCES TABLE
- LEAD CONTACT AND MATERIAL AVAILABILITY
- EXPERIMENTAL MODEL AND SUBJECT DETAILS
 - Electrophysiology experiments
 - Behavioral experiments
 - Immunohistochemistry
- METHOD DETAILS
 - Slice preparation
 - Electrophysiological recordings and analysis
 - Immunohistochemistry
 - Stereotaxic injection
 - Behavioral experiments
 - Post hoc histological analysis
- QUANTIFICATION AND STATISTICAL ANALYSIS
- DATA AND CODE AVAILABILITY

SUPPLEMENTAL INFORMATION

Supplemental Information can be found online at <https://doi.org/10.1016/j.celrep.2019.09.044>.

ACKNOWLEDGMENTS

This work was supported by the Agence Nationale de la Recherche ANR-12-BSV4-0021 (V.C.) and ANR-13-JSV4-0002-01 (R.A.P.), the Ville de Paris Programme Emergences (R.A.P.), and the Institut Universitaire de France (L.V.).

AUTHOR CONTRIBUTIONS

Conceptualization, V.C., R.A.P., and L.V.; Investigation, S.D., V.C., L.T., A.F., R.A.P., and C.C.R.; Formal Analysis, S.D., C.C.R., L.V., R.A.P., and V.C.; Resources, D.M.; Writing, V.C. and R.A.P., with the help of the other authors.

DECLARATION OF INTERESTS

The authors declare no competing interests.

Received: March 3, 2017

Revised: July 31, 2019

Accepted: September 13, 2019

Published: October 29, 2019

REFERENCES

- Ainge, J.A., and Langston, R.F. (2012). Ontogeny of neural circuits underlying spatial memory in the rat. *Front. Neural Circuits* 6, 8.
- Bean, J.C., Lin, T.W., Sathyamurthy, A., Liu, F., Yin, D.-M., Xiong, W.-C., and Mei, L. (2014). Genetic labeling reveals novel cellular targets of schizophrenia susceptibility gene: distribution of GABA and non-GABA ErbB4-positive cells in adult mouse brain. *J. Neurosci.* 34, 13549–13566.
- Berretta, S., Pantazopoulos, H., Markota, M., Brown, C., and Batzianouli, E.T. (2015). Losing the sugar coating: potential impact of perineuronal net abnormalities on interneurons in schizophrenia. *Schizophr. Res.* 167, 18–27.
- Bitanihirwe, B.K.Y., and Woo, T.-U.W. (2014). Perineuronal nets and schizophrenia: the importance of neuronal coatings. *Neurosci. Biobehav. Rev.* 45, 85–99.
- Blakemore, S.-J. (2008). The social brain in adolescence. *Nat. Rev. Neurosci.* 9, 267–277.
- Botcher, N.A., Falck, J.E., Thomson, A.M., and Mercer, A. (2014). Distribution of interneurons in the CA2 region of the rat hippocampus. *Front. Neuroanat.* 8, 104.
- Bozzelli, P.L., Alaiyed, S., Kim, E., Villapol, S., and Conant, K. (2018). Proteolytic Remodeling of Perineuronal Nets: Effects on Synaptic Plasticity and Neuronal Population Dynamics. *Neural Plast.* 2018, 5735789.
- Brückner, G., Grosche, J., Hartlage-Rübsamen, M., Schmidt, S., and Schachner, M. (2003). Region and lamina-specific distribution of extracellular matrix proteoglycans, hyaluronan and tenascin-R in the mouse hippocampal formation. *J. Chem. Neuroanat.* 26, 37–50.
- Buonanno, A. (2010). The neuregulin signaling pathway and schizophrenia: from genes to synapses and neural circuits. *Brain Res. Bull.* 83, 122–131.
- Cabungcal, J.-H., Steullet, P., Morishita, H., Kraftsik, R., Cuenod, M., Hensch, T.K., and Do, K.Q. (2013). Perineuronal nets protect fast-spiking interneurons against oxidative stress. *Proc. Natl. Acad. Sci. USA* 110, 9130–9135.
- Carstens, K.E., Phillips, M.L., Pozzo-Miller, L., Weinberg, R.J., and Dudek, S.M. (2016). Perineuronal Nets Suppress Plasticity of Excitatory Synapses on CA2 Pyramidal Neurons. *J. Neurosci.* 36, 6312–6320.
- Celio, M.R. (1993). Perineuronal nets of extracellular matrix around parvalbumin-containing neurons of the hippocampus. *Hippocampus* 3, 55–60.
- Chen, Y.-J., Zhang, M., Yin, D.-M., Wen, L., Ting, A., Wang, P., Lu, Y.-S., Zhu, X.-H., Li, S.-J., Wu, C.-Y., et al. (2010). ErbB4 in parvalbumin-positive interneurons is critical for neuregulin 1 regulation of long-term potentiation. *Proc. Natl. Acad. Sci. USA* 107, 21818–21823.
- Chevalyere, V., and Piskorowski, R.A. (2016). Hippocampal Area CA2: An Overlooked but Promising Therapeutic Target. *Trends Mol. Med.* 22, 645–655.
- Chevalyere, V., and Siegelbaum, S.A. (2010). Strong CA2 pyramidal neuron synapses define a powerful disinaptic cortico-hippocampal loop. *Neuron* 66, 560–572.
- Chiang, M.-C., Huang, A.J.Y., Wintzer, M.E., Ohshima, T., and McHugh, T.J. (2018). A role for CA3 in social recognition memory. *Behav. Brain Res.* 354, 22–30.
- Del Pino, I., García-Frigola, C., Dehorter, N., Brotons-Mas, J.R., Alvarez-Salvado, E., Martínez de Lagrán, M., Ciceri, G., Gabaldón, M.V., Moratal, D., Dierssen, M., et al. (2013). ErbB4 deletion from fast-spiking interneurons causes schizophrenia-like phenotypes. *Neuron* 79, 1152–1168.
- Dzwonek, J., Rylski, M., and Kaczmarek, L. (2004). Matrix metalloproteinases and their endogenous inhibitors in neuronal physiology of the adult brain. *FEBS Lett.* 567, 129–135.
- Erbs, E., Faget, L., Scherrer, G., Kessler, P., Hentsch, D., Vonesch, J.-L., Matifas, A., Kieffer, B.L., and Massotte, D. (2012). Distribution of delta opioid receptor-expressing neurons in the mouse hippocampus. *Neuroscience* 227, 203–213.
- Evans, P.R., Lee, S.E., Smith, Y., and Hepler, J.R. (2014). Postnatal developmental expression of regulator of G protein signaling 14 (RGS14) in the mouse brain. *J. Comp. Neurol.* 522, 186–203.
- Giedd, J.N., Blumenthal, J., Jeffries, N.O., Castellanos, F.X., Liu, H., Zijdenbos, A., Paus, T., Evans, A.C., and Rapoport, J.L. (1999). Brain development during childhood and adolescence: a longitudinal MRI study. *Nat. Neurosci.* 2, 861–863.
- Hayani, H., Song, I., and Dityatev, A. (2018). Increased Excitability and Reduced Excitatory Synaptic Input Into Fast-Spiking CA2 Interneurons After Enzymatic Attenuation of Extracellular Matrix. *Front. Cell Neurosci.* 12, 149.
- Hensch, T.K. (2005). Critical period plasticity in local cortical circuits. *Nat. Rev. Neurosci.* 6, 877–888.
- Hitti, F.L., and Siegelbaum, S.A. (2014). The hippocampal CA2 region is essential for social memory. *Nature* 508, 88–92.
- Hori-Hayashi, N., Sasagawa, T., Matsunaga, W., and Nishi, M. (2015). Development and Structural Variety of the Chondroitin Sulfate Proteoglycans-Contained Extracellular Matrix in the Mouse Brain. *Neural Plast.* 2015, 256389.
- Iwakura, Y., and Nawa, H. (2013). ErbB1-4-dependent EGF/neuregulin signals and their cross talk in the central nervous system: pathological implications in schizophrenia and Parkinson's disease. *Front. Cell. Neurosci.* 7, 4.
- Karayiorgou, M., Simon, T.J., and Gogos, J.A. (2010). 22q11.2 microdeletions: linking DNA structural variation to brain dysfunction and schizophrenia. *Nat. Rev. Neurosci.* 11, 402–416.
- Kay, K., Sosa, M., Chung, J.E., Karlsson, M.P., Larkin, M.C., and Frank, L.M. (2016). A hippocampal network for spatial coding during immobility and sleep. *Nature* 531, 185–190.
- Knable, M.B., Barci, B.M., Webster, M.J., Meador-Woodruff, J., and Torrey, E.F.; Stanley Neuropathology Consortium (2004). Molecular abnormalities of the hippocampus in severe psychiatric illness: postmortem findings from the Stanley Neuropathology Consortium. *Mol. Psychiatry* 9, 609–620.
- Kogan, J.H., Frankland, P.W., and Silva, A.J. (2000). Long-term memory underlying hippocampus-dependent social recognition in mice. *Hippocampus* 10, 47–56.
- Kohara, K., Pignatelli, M., Rivest, A.J., Jung, H.-Y., Kitamura, T., Suh, J., Frank, D., Kajikawa, K., Mise, N., Obata, Y., et al. (2014). Cell type-specific genetic and optogenetic tools reveal hippocampal CA2 circuits. *Nat. Neurosci.* 17, 269–279.
- Leroy, F., Brann, D.H., Meira, T., and Siegelbaum, S.A. (2017). Input-Timing-Dependent Plasticity in the Hippocampal CA2 Region and Its Potential Role in Social Memory. *Neuron* 95, 1089–1102.e5.
- Megias, M., Emri, Z., Freund, T.F., and Gulyás, A.I. (2001). Total number and distribution of inhibitory and excitatory synapses on hippocampal CA1 pyramidal cells. *Neuroscience* 102, 527–540.
- Mei, L., and Xiong, W.-C. (2008). Neuregulin 1 in neural development, synaptic plasticity and schizophrenia. *Nat. Rev. Neurosci.* 9, 437–452.

- Mietzsch, M., Broecker, F., Reinhardt, A., Seeberger, P.H., and Heilbronn, R. (2014). Differential adeno-associated virus serotype-specific interaction patterns with synthetic heparins and other glyicans. *J. Virol.* *88*, 2991–3003.
- Moy, S.S., Ghashghaei, H.T., Nonneman, R.J., Weimer, J.M., Yokota, Y., Lee, D., Lai, C., Threadgill, D.W., and Anton, E.S. (2009). Deficient NRG1-ERBB signaling alters social approach: relevance to genetic mouse models of schizophrenia. *J. Neurodev. Disord.* *7*, 302–312.
- Nasrallah, K., Piskorowski, R.A., and Chevaleyre, V. (2015). Inhibitory Plasticity Permits the Recruitment of CA2 Pyramidal Neurons by CA3. *eNeuro* *2*, ENEURO.0049-15.2015.
- Oliva, A., Fernández-Ruiz, A., Buzsáki, G., and Berényi, A. (2016). Role of Hippocampal CA2 Region in Triggering Sharp-Wave Ripples. *Neuron* *91*, 1342–1355.
- Pattwell, S.S., Lee, F.S., and Casey, B.J. (2013). Fear learning and memory across adolescent development: Hormones and Behavior Special Issue: Puberty and Adolescence. *Horm. Behav.* *64*, 380–389.
- Piskorowski, R.A., and Chevaleyre, V. (2013). Delta-opioid receptors mediate unique plasticity onto parvalbumin-expressing interneurons in area CA2 of the hippocampus. *J. Neurosci.* *33*, 14567–14578.
- Piskorowski, R.A., Nasrallah, K., Diamantopoulou, A., Mukai, J., Hassan, S.I., Siegelbaum, S.A., Gogos, J.A., and Chevaleyre, V. (2016). Age-Dependent Specific Changes in Area CA2 of the Hippocampus and Social Memory Deficit in a Mouse Model of the 22q11.2 Deletion Syndrome. *Neuron* *89*, 163–176.
- Quock, R.M., Burkey, T.H., Varga, E., Hosohata, Y., Hosohata, K., Cowell, S.M., Slate, C.A., Ehler, F.J., Roeske, W.R., and Yamamura, H.I. (1999). The delta-opioid receptor: molecular pharmacology, signal transduction, and the determination of drug efficacy. *Pharmacol. Rev.* *51*, 503–532.
- Rezaï, X., Faget, L., Bednarek, E., Schwab, Y., Kieffer, B.L., and Massotte, D. (2012). Mouse δ opioid receptors are located on presynaptic afferents to hippocampal pyramidal cells. *Cell. Mol. Neurobiol.* *32*, 509–516.
- Ribak, C.E., Seress, L., and Leranth, C. (1993). Electron microscopic immunocytochemical study of the distribution of parvalbumin-containing neurons and axon terminals in the primate dentate gyrus and Ammon's horn. *J. Comp. Neurol.* *327*, 298–321.
- Scherrer, G., Tryoen-Tóth, P., Filliol, D., Matifas, A., Laustriat, D., Cao, Y.Q., Basbaum, A.I., Dierich, A., Vonesh, J.-L., Gavériaux-Ruff, C., and Kieffer, B.L. (2006). Knockin mice expressing fluorescent delta-opioid receptors uncover G protein-coupled receptor dynamics in vivo. *Proc. Natl. Acad. Sci. USA* *103*, 9691–9696.
- Soleman, S., Filippov, M.A., Dityatev, A., and Fawcett, J.W. (2013). Targeting the neural extracellular matrix in neurological disorders. *Neuroscience* *253*, 194–213.
- Stevenson, E.L., and Caldwell, H.K. (2014). Lesions to the CA2 region of the hippocampus impair social memory in mice. *Eur. J. Neurosci.* *40*, 3294–3301.
- Vullhorst, D., Neddens, J., Karavanova, I., Tricoire, L., Petralia, R.S., McBain, C.J., and Buonanno, A. (2009). Selective expression of ErbB4 in interneurons, but not pyramidal cells, of the rodent hippocampus. *J. Neurosci.* *29*, 12255–12264.
- Wersinger, S.R., Ginns, E.I., O'Carroll, A.-M., Lolait, S.J., and Young, W.S., 3rd. (2002). Vasopressin V1b receptor knockout reduces aggressive behavior in male mice. *Mol. Psychiatry* *7*, 975–984.
- Woo, R.-S., Li, X.-M., Tao, Y., Carpenter-Hyland, E., Huang, Y.Z., Weber, J., Neiswender, H., Dong, X.-P., Wu, J., Gassmann, M., et al. (2007). Neuregulin-1 enhances depolarization-induced GABA release. *Neuron* *54*, 599–610.
- Yamada, J., and Jinno, S. (2013). Spatio-temporal differences in perineuronal net expression in the mouse hippocampus, with reference to parvalbumin. *Neuroscience* *253*, 368–379.
- Zhao, M., Choi, Y.-S., Obrietan, K., and Dudek, S.M. (2007). Synaptic plasticity (and the lack thereof) in hippocampal CA2 neurons. *J. Neurosci.* *27*, 12025–12032.

STAR★METHODS

KEY RESOURCES TABLE

REAGENT or RESOURCE	SOURCE	IDENTIFIER
Antibodies		
Wisteria Floribunda Agglutinin (WFA)-biotinylated	Sigma Aldrich	L1516-2mg lot#SLBL4991V
Rabbit anti-parvalbumin antibody	Swant	PV27; RRID: AB_2631173
Mouse monoclonal HER-4 antibody	Invitrogen	Catalog # MA5-12888 lot#RG2240715; RRID: AB_10986112
Mouse monoclonal anti-RGS14 antibody	Neuromab	catalog # 75-170 (RRID: AB_2179931)
Polyclonal chicken anti-GFP antibody	Abcam	Ab13970, lot:GR236651-10; RRID: AB_300798
Rabbit polyclonal anti-purkinje cell protein 4 (PCP4)	Santa Cruz	Cat# sc-74816; RRID: AB_2236566
Donkey anti-Rabbit IgG (H+L) Highly Cross-Absorbed Secondary Antibody, Alexa Fluor 647	ThermoFisher Scientific	Cat# A-31573; RRID: AB_2536183
Alexa-546 streptavidin conjugate	Life Technologies	S11225 lot#1873983; RRID: AB_2532130
Alexa-647 streptavidin conjugate	Life Technologies	S21374 lot#1596042; RRID: AB_2336066
Dylight 549 Strepavidin	Vector Labs	Cat# SA-5549; RRID: AB_2336408
Cy3 tagged goat anti-rabbit	Jackson ImmunoResearch	RRID: AB_2338000
Alexa-647 goat anti-mouse	Life Technologies	Cat # A21240 lot#1885955; RRID: AB_2335809
Alexa 488 goat anti-chicken	Life Technologies	A11039 lot#1812246; RRID: AB_2534096
Bacterial and Virus Strains		
AAV serotype 5 virus expressing GFP-tagged cre recombinase	University of North Carolina Vector Core	Serotype 5, AAV-CMV-cre-GFP
AAV serotype 5 virus expressing GFP used as control virus expressing GFP	University of North Carolina Vector Core	Serotype 5, AAV-CMV-GFP
Chemicals, Peptides, and Recombinant Proteins		
rhMRG1-β1/HRG1-β1 EGF domain	R&D Systems	Cat# 396-HB/CF lot ACD1514072
Chondroitinase ABC from <i>Proteus vulgaris</i>	Sigma-Aldrich	Cat# C3667
CGP 55845 hydrobromide	Tocris	Cat# 1248 10mg batch: 6A/149745
SR 95531 hydrobromide	Tocris	Cat# 1262 10mg bact:10A/150171
AG1478- ErbB4 antagonist	Tocris	Cat# 1276 lot 2A/191529
PKI 14-22 amide, myristoylated	Tocris	Cat# 2546 batch 6B,C
D-AP5	Hello bio	HB0225-100mg batch:E0267-4-1
DPDPE	TOCRIS	Cat#1431/1mg batch:9A, 10A, 11A,
NBQX	Hello bio	HB0225-100mg batch E0714-4-2
Experimental Models: Organisms/Strains		
Mouse model: C57BL/6J	Janvier Labs	N/A
Mouse model: C57BL/6S _{JL}	Charles River France	N/A
Mouse model: DOR-flox (Orpd1 ^{fl/fl}) Mouse model: DOR-EGFP	Dominique Massotte, CNRS UPR3212, Team Neuroanatomy, pain & psychopathologies	N/A
Software and Algorithms		
ImageJ- Used for all image analyzing and quantification	ImageJ	https://imagej.net/Welcome
Axograph X software for data acquisition	Axograph	https://axograph.com
pClamp10- data acquisition	Molecular devices	https://www.moleculardevices.com
Origin Pro- data analysis	Origin Lab	https://www.originlab.com
GraphPad Prism version 6.00 for Mac OS	GraphPad Software	https://www.graphpad.com

LEAD CONTACT AND MATERIAL AVAILABILITY

Further information and requests for resources and reagents should be directed to and will be fulfilled by the Lead Contact, Vivien Chevalleyre (vivien.chevalleyre@parisdescartes.fr). This study did not generate new unique reagents.

EXPERIMENTAL MODEL AND SUBJECT DETAILS

Electrophysiology experiments

All experiments were performed on C57B6 male mice.

Behavioral experiments

C57B6J male mice (Charles River, France) were used for behavioral experiments. They were housed in groups of five since weaning at P21 in standard breeding cages with food and water *ad libitum*, and were placed at a constant temperature ($23 \pm 1^\circ\text{C}$) under diurnal conditions (light-dark: 8:00AM–8:00PM). Mice were tested during the first half of the light period.

Immunohistochemistry

Histology experiments were performed on wild-type C57BL/6J or on DOR-EGFP mice.

METHOD DETAILS

Slice preparation

400 μm transverse hippocampal slices were prepared from C57BL/6Rj male mice. Animals were euthanized in accordance with institutional regulations under anesthesia with isoflurane. Hippocampi were removed and placed upright into an agar mold and cut with a vibratome (Leica VT1200S, Germany) in ice-cold solution containing (in mM): 10 NaCl, 195 sucrose, 2.5 KCl, 15 glucose, 26 NaHCO₃, 1.25 NaH₂PO₄, 1 CaCl₂ and 2 MgCl₂. The slices were then transferred to 30°C artificial cerebral spinal fluid (ACSF), (in mM: 125 NaCl, 2.5 KCl, 10 glucose, 26 NaHCO₃, 1.25 NaH₂PO₄, 2 Na Pyruvate, 2 CaCl₂ and 1 MgCl₂) for 30 min and kept at room temperature for at least 1.5 hr before recording. For experiments using digestion of the PNN, slices were further incubated in a separate chamber with either Chondroitinase ABC (2 U / mL; Sigma) and 0.1% bovine serum albumin (BSA) in ACSF, or with 0.1% BSA in ACSF for 2 hours. All experiments were performed at 33°C.

Electrophysiological recordings and analysis

Whole-cell recordings were obtained from CA2 PNs in voltage clamp mode with a patch pipette (3–5 M Ω) containing (in mM): 135 CsMethylSulfate, 5 KCl, 0.1 EGTA-Na, 10 HEPES, 2 NaCl, 5 ATP, 0.4 GTP, 10 phosphocreatine; pH 7.2; 280–290 mOsm). Series resistance (typically 12–18 M Ω) was monitored throughout each experiment and cells with more than 15% change were excluded from analysis. Before beginning whole cell experiments, we identified the CA2 PNs by somatic location and size. Furthermore, the cell type was confirmed by several electrophysiological properties as previously described (Chevalleyre and Siegelbaum, 2010). Cells were also filled with biocytin and post hoc labeling of filled cells and imaging was performed to confirm CA2 recording when necessary.

Synaptic currents were evoked by mono-polar stimulation with a patch pipette filled with ACSF and positioned in the middle of CA1 SR. The amplitudes of the IPSCs were normalized to the baseline amplitude. A HFS (100 pulses at 100Hz repeated twice, 20 s apart) was applied following stable baseline. The magnitude of plasticity was estimated by comparing averaged responses at 30–40 min after the induction protocol with baseline-averaged responses from 0 to 10 min before the induction protocol. We used pClamp10 and Axograph X software for data acquisition and Origin Pro for data analysis. Statistical comparisons were performed using Student's t test, ANOVA, Wilcoxon, Mann-Witney or Kruskal-Wallis where appropriate. All drugs were bath-applied following dilution into the external solution from concentrated stock solutions. Results are reported as mean \pm SEM.

Immunohistochemistry

For histology experiments, wt C57BL/6J at P17, P22, P29, P35 and P50 were anesthetized according to institutional regulation and transcardially perfused with ice-cold phosphate-buffered saline (PBS) followed by 4% paraformaldehyde in PBS. DOR-EGFP mice were anesthetized with pentobarbital and perfused with ice-cold 4% paraformaldehyde at 20 ml/min for 5 min. The brains were dissected, post-fixed and 30 μm floating coronal sections were prepared with a Leica 1000S vibratome. 8 serial sections were selected spanning bregma -1.8 to -2.1 . Sections were permeabilized in PBS + 0.2% Triton, followed by incubation in blocking solution (PBS+0.2% Triton + 3% normal goat serum). Primary antibody incubation was carried out in blocking solution overnight at 4°C. A rabbit anti-parvalbumin antibody (Swant) was used at a dilution of 1:2000, the mouse monoclonal anti-RGS14 antibody (Neuromab) was used at dilution of 1:300. GFP-DOR signal was amplified with a polyclonal chicken anti-GFP (Abcam) at a dilution of 1:10000, and ErbB4 was stained with the mouse monoclonal HER-4 antibody (Invitrogen) at a dilution of 1:300. The PNN was

stained with Wisteria Floribunda Agglutinin (WFA)-biotinylated (Sigma) diluted at 1:1,000 followed by either alexa-555 streptavidin (Life Technologies) or alexa-647 streptavidin (Life Technologies) diluted at 1:500. Secondary antibodies were carried out in block solution for 4 hours. Secondary antibodies were Cy3 tagged goat anti-rabbit (Jackson ImmunoResearch), alexa-647 tagged goat anti-mouse (Life Technologies), Alexa 488 rat anti-chicken (Life Technologies) all diluted at 1:800.

Images were collected with a Zeiss 710 laser-scanning confocal microscope. Z series images consisting of three channels were collected every 0.9 μm over a total distance of 30 μm per slice. RGS14 staining alone was used to define area CA2. All image analysis and quantification was performed with ImageJ.

Stereotaxic injection

For PNN degradation, male mice (7–8 weeks old, Charles River, France) were anaesthetized with isoflurane (2%–5%) and placed in a stereotaxic apparatus (Kopf). Each mouse was submitted to two bilateral injections into the area CA2 of dorsal hippocampus (–1.1 mm anteroposterior, \pm 0.6 mm mediolateral and –2.00 mm dorsoventral, and –1.98 mm anteroposterior, \pm 2.3 mm mediolateral and –2.05 mm dorsoventral, relative to bregma) of 100 nL of a solution with ChABC (50 U/ml, Sigma, $n = 12$ mice), or a vehicle solution (phosphate buffer saline 0.1 M, PBS, $n = 10$ mice). Lidocaine was applied on the flesh before suturing the skin. The animals were then allowed to recover for a week before behavioral testing. To selectively knockout DOR in area CA2, DOR-flox mice (line *Orpd1^{fl/fl}*, REF) were submitted to two bilateral injections into area CA2 of 100 nL of rAAV5-hSyn-eGFP or rAAV5-hSyn-Cre-eGFP solution. Lidocaine was applied on the flesh before suturing the skin. The animals were submitted to behavioral testing 6 weeks after viral injection.

Behavioral experiments

A total of 40 C57BL/6J male mice (Charles River, France) were used for behavioral experiments. They were housed in groups of five since weaning at P21 in standard breeding cages with food and water *ad libitum*, and were placed at a constant temperature ($23 \pm 1^\circ\text{C}$) under diurnal conditions (light-dark: 8:00AM–8:00PM). Mice were tested during the first half of the light period, and the experiments were performed in strict accordance with the recommendations of the European Union (86/609/EEC) and the French National Committee (87/848). For five-trial social memory test (Kogan et al., 2000), each mouse was first placed for 10 min habituation in a large chamber (25x35 cm) with an empty cylindrical small cage placed in the center (8 cm diameter). Then a stimulus mouse, from same age and sex, but never encountered before, was introduced in the small cage for four successive trials of 5 min (ITI 10 min). On the fifth trial, a novel stimulus mouse was introduced. The direct interactions were scored online by the experimenter. All apparatuses and testing chambers were cleaned with 70% ethanol between animals. Mice were sacrificed 3 hours after the social memory test.

Locomotor activity was analyzed during the habituation session of the novel object location task (see below). Each animal was allowed to explore a circular open-field (62 cm diameter, 40 cm-high wall) for 10 minutes. The distance moved in the open field was measured by means of video tracking software (EthoVision XT, Noldus).

The object location test addresses the ability of mice to discriminate between a novel and a familiar spatial location in an open-field with a visual cue (striped pattern). During acquisition, two identical objects were placed in the middle of the open-field. The mice were allowed to explore for 10 min during which the time spent exploring the two objects was recorded. In the test phase held 3 hours later, identical copies of the sample objects were exposed and one of the two objects was moved to a novel location. The position (left or right) of the displaced object was chosen pseudorandomly to reduce bias toward a particular position. Mice were allowed to explore the objects during 10 min. All apparatuses and testing chambers were cleaned with 70% ethanol between animals.

Post hoc histological analysis

Mice were administered pentobarbital before being flush-perfused transcardially with normal saline for 45–60 s. The brains were removed and bisected, then drop-fixed in 4% PFA/PB 0.1M for 48 hours at 4°C , and transferred into a 30% sucrose solution with 0.1% sodium azide for at least 2 days. Coronal sections of 30 μm were prepared with a sliding microtome (Leica SM2010R) equipped with a freezing stage (Physitemp BFS-3MP). A series of free-floating sections, from bregma –0.6 to –3.0 and of 150 μm apart, was used for PCP4 and WFA stainings. Sections were rinsed extensively in PBS with 0.25% Triton X-100 (PBST) before being placed for 15 min in a PBS solution with 3% H₂O₂ and 10% methanol. After two washes in PBST, the sections were transferred in a 10% normal donkey serum (NDS) in PBST blocking solution for 1 hour. The sections were then incubated overnight at room temperature in a PBST/10% NDS solution containing the rabbit anti-PCP4 antibody (Santa Cruz; 1:250) and the Wisteria Floribunda Agglutinin (WFA)-biotinylated (Sigma; 1:1,000). The next day, sections were incubated for 90 min in a PBST/10% NDS solution with secondary antibody donkey anti-rabbit Alexa 647 (Molecular Probes; 1:250) and streptavidin-TRITC (Molecular Probes; 1:500). For histological control of injections and measurements of PNN degradation, 4 hemi-sections were analyzed per animal. PCP4 staining was used to define area CA2. Images were collected with a Leica DM600B fluorescence microscope, and image analysis and quantification were performed with ImageJ and Fiji plugin.

QUANTIFICATION AND STATISTICAL ANALYSIS

We used pClamp10 and Axograph X software for data acquisition and Origin Pro and GraphPad Prism for data analysis. Statistical comparisons were performed using Student's t test and ANOVA. When the distribution was not normal, we used non-parametric test (Wilcoxon and Mann-Whitney test, see [Table S1](#)). Statistical significance was set to $p < 0.05$ (** indicates $p < 0.001$, * indicates $p < 0.01$, * indicates $p < 0.05$). Data are reported as mean \pm SEM. Error bars shown in figures represent SEM.

DATA AND CODE AVAILABILITY

This study did not generate datasets and code.